Hydrogenases

DOI: 10.1002/anie.201209063

The Structural Plasticity of the Proximal [4Fe3S] Cluster is Responsible for the O_2 Tolerance of Membrane-Bound [NiFe] Hydrogenases**

Jean-Marie Mouesca, Juan C. Fontecilla-Camps, and Patricia Amara**

Hydrogen metabolism is restricted to three classes of enzymes, [NiFe], [FeFe], and [Fe] hydrogenases.[1] As H_2 oxidation catalysts, [NiFe] hydrogenases are competitive with the more expensive Pt.[2] Consequently, there has been a significant effort to understand the H_2 uptake/evolution mechanism for its application in hydrogen-based technologies.[3] These enzymes are sensitive to oxygen; an exception is a subclass of periplasmic membrane-bound [NiFe] hydrogenases represented by *Ralstonia eutropha* (*Re*MBH),[4] *Escherichia coli* hydrogenase 1 (*Ec*Hyd-1),[5] and *Aquifex aeolicus* hydrogenase 1 (*Aa*Hase-1).[6] This O_2-tolerant subclass has already been used in potentially relevant technological applications.[7] [NiFe] designates the active site, which is located in the large subunit and consists of a bimetallic NiFe center coordinated by four cysteine residues and CO/CN^- ligands to Fe.[8] Upon oxidation, two EPR-active redox states are detected in standard (i.e., O_2-sensitive) hydrogenases, called Ni-A and Ni-B. The Ni-B species, characterized by a Ni^{III}-Fe^{II} center with a bridging hydroxide ion,[9] is a "ready" state, as it reactivates rapidly under reducing conditions.[4,8b] Conversely, the Ni-A state, a Ni^{III}-Fe^{II} center with most probably a bridging (hydro)peroxo,[9] is "unready" and requires prolonged reactivation, which may not be achievable in vivo. EPR and FTIR studies on *Re*MBH[10] and *Aa*Hase-1[6] have shown that, with the exception of the Ni-A species, most redox states observed in standard hydrogenases are also observed in these O_2-tolerant enzymes. In standard hydrogenases, electron transfer is ensured by proximal and distal (relative to the active site) [4Fe4S] clusters and a medial [3Fe4S] cluster.[8a] Unexpectedly, an EPR study on *Re*MBH recorded a putative additional paramagnetic species at a fixed redox potential of $+290$ mV, coupled to both the active site and the medial cluster. This observation suggested the presence of a modification near or at the proximal cluster,[10] as further confirmed by an X-ray absorption spectroscopy study.[11] Furthermore, assuming a proximal [4Fe4S] cluster, redox potentials for $+2/+1$ and $+3/+2$ transitions were determined at $-60/+160$ mV and $+98/+232$ mV for *Re*MBH[12] and *Aa*Hase-1,[13] respectively. The narrow potential difference of less than 220 mV between these two redox couples has been recently also observed in *Ec*Hyd-1.[14] Notably, the nonphysiological superreduction to the $+1$ state of high-potential iron–sulfur protein (HiPIP) $[4Fe4S]^{3+}$ cluster occurs at a potential that is about 1000 mV more negative than that of the $+3/+2$ redox couple.[15] The possible $+3/+2$ superoxidation of the proximal cluster in O_2-tolerant [NiFe] hydrogenases was thus proposed to be a redox switch against oxidative stress.[13] One specificity of these enzymes is the presence of two supernumerary conserved cysteine residues (Cys19 and Cys120 in *Ec*Hyd-1) close to the proximal cluster.[10] Site-directed mutagenesis studies indicated that these residues are essential for the unusual redox property of this cluster and the associated O_2 tolerance.[16] Recently, the crystal structures of oxidized and H_2-reduced forms of *Hydrogenovibrio marinus* (*Hm*) MBH[17] and of the reduced form of *Re*MBH[18] showed that the highly symmetrical four-cysteine-coordinated [4Fe4S] cluster in standard hydrogenases is substituted by a [4Fe3S] cluster. Remarkably, the absent sulfide is replaced by both the bridging Cys19 thiolate and the terminally bound Cys120, which coordinates a Fe atom also bound to another cysteine thiolate. This results in an unprecedented asymmetric FeS cluster, which is further deformed upon superoxidation as the Fe that is coordinated by Cys19 and Cys20 moves away from the remaining [3Fe3S] moiety and binds the deprotonated amide nitrogen atom of Cys20.[17] We reported the crystal structures of the as-isolated and H_2-reduced *Ec*Hyd-1, and proposed that a glutamate residue conserved in O_2-tolerant hydrogenases (Glu76 in *Ec*Hyd-1) plays the role of the base that deprotonates the amide moiety and allows the formation of the Fe–N bond.[19] Herein, we call the three redox states of the reduced $[4Fe3S]^{3+}$, oxidized $[4Fe3S]^{4+}$, and superoxidized proximal $[4Fe3S]^{5+}$ clusters PC1, PC2, and PC3, respectively (Table 1). Previously,[19] we reported quantum calculations that defined an electronic/spin state for the PC3 species and fitted available structural and spectroscopic data.[13] In the present study, we examined the remarkable plasticity of the [4Fe3S] cluster in the PC2/PC3 transition with special attention to the role of Glu76. We found that the interplay between the high asymmetry of the cluster and the resulting Fe valence/spin localization in the three redox states is the key feature that explains the facile superoxidation.

[*] Dr. J. C. Fontecilla-Camps, Dr. P. Amara
Metalloproteins Unit, Institut de Biologie Structurale J.P. Ebel
Commissariat à l'Énergie Atomique, Centre National de la Recherche Scientifique, Université Joseph Fourier
41 rue Jules Horowitz, 38027 Grenoble (France)
E-mail: juan.fontecilla@ibs.fr
patricia.amara@ibs.fr

Dr. J.-M. Mouesca
Laboratoire de Chimie Inorganique et Biologique UMR-E 3 CEA-UJF
Institut de Nanosciences et Cryogénie, CEA-Grenoble
17 avenue des Martyrs, 38054 Grenoble (France)

[**] We thank Drs David Rinaldo and Anne Volbeda for helpful discussions. We appreciate the help from the staff of the computing facility provided by the Commissariat à l'Energie Atomique (CEA/DSV/GIPSI), Saclay, and CCRT, Bruyères-le-Châtel, and thank the CEA and CNRS for institutional funding.

Supporting information for this article is available on the WWW under http://dx.doi.org/10.1002/anie.201209063.

Table 1: Notation for the different redox states/charges and spin states of the proximal cluster investigated in this study and the corresponding number of mixed-valence (*mv*) pairs.

	Reduced PC1					Oxidized PC2					Superoxidized PC3				
[4Fe4S]		+1					+2					+3			
[4Fe3S]		+3					+4					+5			
mv pairs		1					2					1			
		Fe1	Fe2	Fe3	Fe4		Fe1	Fe2	Fe3	Fe4		Fe1	Fe2	Fe3	Fe4
spin states[a]	BS24	−4/2	+5/2	***−4/2***	+4/2	BS13	−4/2	+5/2	***−5/2***	***+4/2***	BS13*[b]	−4/2	+5/2	−5/2	***+5/2***
	BS12	−4/2	−5/2	+4/2	+4/2	BS12	−4/2	−5/2	+5/2	+4/2					
	BS13	+4/2	−4/2	+5/2	−4/2	BS14	−4/2	+5/2	+4/2	−5/2					

[a] Changes upon the first (italicized, bold) and second (bold) oxidation are indicated in the favored states. [b] BS13* was found to be the favored state for PC3.[19]

We have investigated the Glu76 protonation state in PC2, followed by Cys20 amide deprotonation and PC2/PC3 cluster oxidation. The geometry of the oxidized PC2 state with a protonated Glu76 was optimized by employing hybrid quantum mechanical/molecular mechanical potentials.[20] The three possible arrangements of iron spin pairs, namely BS12, BS13, and BS14 (see Table 1 and the Supporting Information for details) led to models that were very similar to the as-isolated *Ec*Hyd-1 initial conformation (pdb code 3USE),[19] regardless of the DFT method that was used. Once Glu76 was deprotonated, a gradually tuning of the amount of Hartree–Fock (HF) potential from 5%[21] to 20% (more ionicity) within the DFT method revealed the surprising mobility of the unique Fe4, which was loosely coordinated by Cys20 and the supernumerary Cys19 (Figure 1). Above 10% HF potential, Fe4 moves toward the amide moiety of Cys20 (Fe4* position in Figure 1) to a position close to the one it adopts in the PC3 X-ray model (Fe4** in Figure 1B). This movement was also observed when the M06 functional, developed for organometallic and inorganometallic chemistry, was used.[22] Glu76 deprotonation therefore triggers the displacement of Fe4, which further acidifies the amide proton of Cys20, thus resulting in deprotonation of the amide moiety (see below). For all calculations, we started from the Glu76 conformation most distant from the [4Fe3S] core (Figure 1), as it is common to all crystal structures.[17–19] Although crystallography of *Ec*Hyd-1 identified two conformations for this residue,[19] geometry optimizations of PC2 favor the farthest position, regardless of the protonation state. In reality, the protonation states will change as Glu76 interacts with Glu16, the first residue in the proposed proton pathway, which, in turn, will change the conformations of the side chains of the remaining residues in the pathway.[8b]

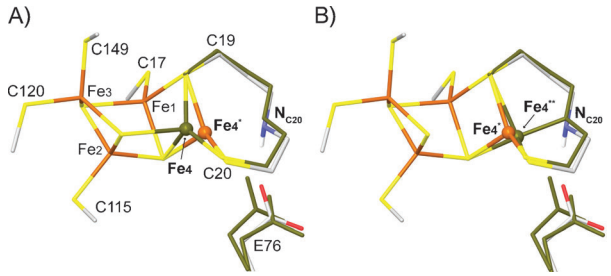

Figure 1. Optimized structure of the PC2-BS13 state represented in standard atom color codes superimposed with the X-ray models of A) PC2 in the as-isolated *Ec*Hyd-1, and B) PC3 in the as-isolated *Ec*Hyd-1.[19] The parts of the X-ray conformations that are different from our optimized model are shown in dark green. Fe4, Fe4*, and Fe4** are the unique iron atoms in the PC2, PC2-BS13 model from calculations, and PC3 X-ray model, respectively.

The Fe4 displacement was observed in both oxidized PC2-BS12 and PC2-BS13 states, but not in PC2-BS14, in which this iron stays in its initial position (Fe4 in Figure 1A and Table S1 in the Supporting Information). Interestingly, orbital analyses show that Fe4 is strictly ferrous in the BS12 and BS13 states, but ferric in BS14 (Table S2). In our previous study of *Ec*Hyd-1, we determined that, based on the available spectroscopic and structural data, BS13 is the best model for the superoxidized state PC3 (Table 1).[19] Therefore, we first tried to oxidize PC2-BS13 to PC3-BS13 in its initial conformation and then to optimize its geometry. But Fe4, being ferric (as in PC2-BS14), does not move toward the Cys20 amide moiety, thus precluding its acidification and deprotonation.[23] We conclude that a ferrous Fe4 in both the PC2-BS12 and PC2-BS13 states[24] should be a requirement to elicit the superoxidation. However, PC2-BS12 can be ruled out because spectroscopic parameter calculations[19] on its corresponding PC3-BS12 state did not fit *Aa*Hase-1 experimental Mössbauer data.[13] Subsequently, we investigated whether the superoxidation or the proton transfer from the amide moiety to Glu76 occurs next, that is, after the ferrous Fe4 has moved toward the backbone amide nitrogen. Scanning of the potential energy surface for the proton transfer in the oxidized (PC2, ferrous Fe4) or superoxidized (PC3, ferric Fe4) state indicates that the transfer is clearly favored in the former state with a barrier of about 5 kcal mol^{-1}, which is twice as low as the one computed for the latter state (Table S3). Hence, we propose that proton transfer in PC2-BS13 occurs first, immediately[25] followed by superoxidation to PC3-BS13, thus allowing the formation of the stabilizing Fe4(III)–N bond (Table S3). The proton is further transferred to the second oxygen atom of the carboxylate of Glu76, which interacts with Glu16, the first residue in the proton relay pathway. It should be noted that in the PC3-BS13 structure obtained from PC2-BS13, there is no Fe–O_{E76} bond (Table S3). Conversely, a Fe–O bond between the Fe,

corresponding to Fe4, and the carboxylate of Asp75 (equivalent to Glu76) was observed in the proximal cluster of the O_2-sensitive hydrogenase from *Allochromatium vinosum*.[26] The authors suggested that the cubane was distorted as a result of the reduction by X-ray-induced photoelectrons. Although Fe moves toward Asp75, the whole arrangement is very different from the one we observed in PC3.

The three-dimensional structures showed that the main difference between O_2-sensitive and O_2-tolerant hydrogenases lies in the architecture of the proximal FeS cluster (Figure 2). In the former, this center is a standard cuboidal

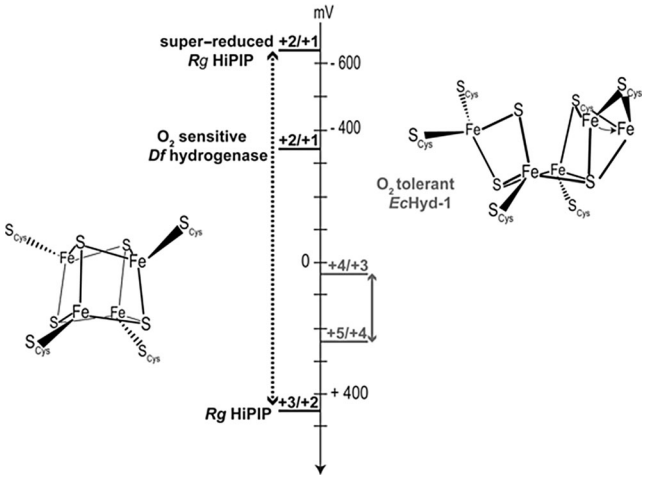

Figure 2. Differences of redox potentials. Left: symmetrical [4Fe4S]-$(Cys)_4$ cluster with the $+3/+2$ and nonphysiological $+2/+1$ redox couples in HiPIP of *Rhodopila globiformis* (*Rg*).[15b] Reference: $+2/+1$ redox couple in O_2-sensitive hydrogenase from *Desulfovibrio fructosovorans* (*Df*).[28] Right: asymmetrical [4Fe3S]$(Cys)_6$ cluster with the equivalent $+5/+4$ and $+4/+3$ redox couples in *Ec*Hyd-1.[14]

$[4Fe4S](Cys)_4$ cluster that is symmetrically arranged. From a redox perspective, such a cluster can in principle function between three redox states. The $1+$ and $2+$ states usually operate at low redox potentials of $-600/-400$ mV, such as in bacterial ferredoxins[27] or O_2-sensitive hydrogenases.[28] Conversely, HiPIPs operate between the $+2$ and $+3$ redox states, with a positive redox potential of up to 450 mV[15] (Figure 2, left).

Several contributions to the modulation of redox potentials, such as charges of the local environment, solvent accessibility, hydrogen bonds to the FeS cluster, and thiolate/sulfides ratio, have been considered for iron–sulfur clusters of various nuclearities and redox states.[15b,27,29] One key issue, often overlooked when explaining the large potential gap between the $[4Fe4S]^{+2/+1}$ and $[4Fe4S]^{+3/+2}$ redox couples in HiPIP (Figure 2, left) as opposed to the narrow difference observed for the O_2-tolerant proximal cluster (Figure 2, right), is related to the degree of electronic/spin delocalization that occurs within mixed-valence iron pairs.[29a,c] What follows is a simplified presentation of the main factor that determines the redox potential within FeS clusters (for a more detailed discussion, see references [30] and [31]). Each time full electronic delocalization occurs within a single mixed-valence pair, turning the pair from localized Fe^{3+}-Fe^{2+} to delocalized $Fe^{2.5+}$-$Fe^{2.5+}$, the bonding energy E of the corresponding [4Fe4S] cluster is stabilized by about 350 mV ($E^{deloc} = E^{loc} - 350$).[30] In Table 2, the effect of

Table 2: Contribution of delocalization, which is proportional to the number of delocalized mixed-valence (*mv*) pair(s) in the FeS cluster, to the stabilization energy of the O_2-sensitive and O_2-tolerant proximal cluster. The latter cluster is found to be fully localized for all redox states (i.e., no stabilization energy). These are DFT-computed values with an uncertainty range of ± 50 mV (depending on the exchange-correlation potential). The redox states are indicated in parentheses.

Stabilization energy[a] [mV]	Reduced	Oxidized	Superoxidized
mv pairs	1	2	1
O_2-sensitive $[4Fe4S](SCys)_4$	≈ -350 $(+1)$	≈ -700 $(+2)$	≈ -350 $(+3)$
O_2-tolerant $[4Fe3S](SCys)_6$	≈ 0 $(+3)$	≈ 0 $(+4)$	≈ 0 $(+5)$

[a] Stabilization energy as a result of delocalization.

electronic delocalization is compared for the reduced, oxidized, and superoxidized states ($1+$, $2+$, and $3+$ for the [4Fe4S] cluster and $3+$, $4+$, and $5+$ for the [4Fe3S] cluster). In [4Fe4S] clusters, the $1+$ and $3+$ redox states contain one delocalized pair, and the $2+$ state contains two such pairs. Strikingly, in [4Fe3S] clusters, the three redox states favored by our calculations are found to be fully localized (see the orbital analysis in the Supporting Information).

The potential E^0 of a given redox pair is computed as the difference between the two redox-state energies: $E^0 = E(\text{ox}) - E(\text{rd})$. For standard [4Fe4S] clusters, the electronic delocalization contribution to the $(2+/1+)$ redox pair is therefore negative at approximately -350 mV (Table 2). The same contribution to the $(3+/2+)$ redox pair is positive at approximately $+350$ mV. Thus, besides other effects on redox potentials,[27,29b] electronic delocalization within mixed-valence pair(s) is at the origin of an approximately 700 mV contribution to the gap between the $(2+/1+)$ and $(3+/2+)$ redox pairs (Figure 2, left). As a consequence, in the case of O_2-sensitive hydrogenases, once the first electron is released from the symmetrical $[4Fe4S](Cys)_4$ cluster ($1+ \rightarrow 2+$), the gap for a second oxidation ($2+ \rightarrow 3+$) is energetically unfavorable. Considering the asymmetrical $[4Fe3S](Cys)_6$ cluster, it is remarkable that the three redox states have been computationally found to consist only of valence-localized Fe^{III} and Fe^{II} ions (see Table S3 in the Supporting Information). Therefore, as a first approximation, there will be no significant delocalization contribution to $E^0(4+/3+)$ and $E^0(5+/4+)$. The resulting absence of a potential gap between the two redox pairs in the asymmetrical proximal $[4Fe3S](Cys)_6$ cluster allows the second oxidation to occur (Figure 2, right).

The protection against O_2-induced oxidative stress is thought to reside in the ability of the proximal cluster to rapidly provide two successive electrons to the active site.[13] Under physiological conditions, *Ec*Hyd-1 is most probably in

a reduced state, either Ni-L* or the one more electron reduced Ni-R (see the Supporting Information and Scheme 1). Both states have also been observed in *Re*MBH.[10] Moreover, the standard Ni-C state, with a more labile hydride, and the Ni-R species have been detected in *Aa*Hase-1.[6,32] The immediate availability of four electrons, two from the active site and two from the proximal cluster, prevents the accumulation of the Ni-A state with a partially reduced oxygenated species.[9] Indeed, the Ni-A species is not generated upon O_2 exposure in O_2-tolerant hydrogenases.[6,10] A possible defense mechanism against oxidative stress (Scheme 1) takes all our results into account: 1) O_2 binds either Ni-C-H^- or Ni-L* (state **1**) and forms a (hydro)peroxo species **2**; in the former case the reaction could involve the insertion of molecular oxygen to the nickel–hydride bond;[33] 2) The first electron from the PC1 to PC2 oxidation, as well as a proton from Glu76, lead to species **3**. In the case of O_2-sensitive hydrogenases, **3** further rearranges to the unready Ni-SU state **4′** and oxidizes to Ni-A **5′**. In O_2-tolerant hydrogenases, the deprotonation of Glu76 causes the unique iron to move toward the amide moiety of Cys20, leading to N pyramidalization[24] and acidification of the amide proton.[23] This, in turn, allows the deprotonation of the amide moiety of Cys20 and subsequent superoxidation of PC2 to PC3. The extra proton and electron permit the total reduction of O_2 to H_2O, ultimately leading to the ready Ni-B state **4**.

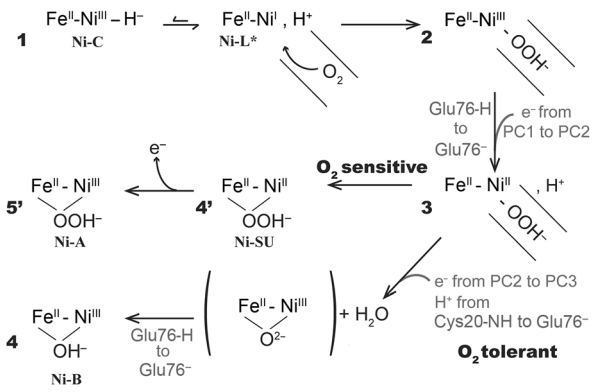

Scheme 1. Proposed reaction mechanism against O_2-induced oxidative stress at the active site of hydrogenases. The 4' and 5' species are depicted with bridging peroxides, which could also be OH^-/SO.[8b] The active site is represented by the bimetallic center, and events that occur at the proximal cluster are shown in gray.

Taken together, the available experimental data indicate that the critical difference between O_2-sensitive and O_2-tolerant hydrogenases resides neither in the active site, nor in the hydrophobic channels that transport H_2/O_2, but rather in the unusual proximal [4Fe3S] cluster.[13,16b,17–19] Here, we have shown that the asymmetric configuration of the O_2-tolerant hydrogenase-proximal cluster, which results from ligation by the two supernumerary Cys residues that replace a sulfide ion, leads to Fe valence localization in the three redox states. Interestingly, an equivalent breakdown of electronic symmetry may be responsible for the defense against oxidative stress provided by the [NiFe] hydrogenase Hya in the bacterium *Geobacter sulfurreducens*.[34] Indeed, in this enzyme, an aspartate residue (a ligand known to engender Fe valence localization in FeS clusters)[29c] replaces a cysteine residue as a ligand of its proximal cluster. The aspartate ligation is then most likely responsible for the unusual redox properties of the Hya proximal cluster.[35] We have previously proposed that in *Ec*Hyd-1 and related enzymes, Glu76 is the base that deprotonates the amide moiety of Cys20.[19] Here, we confirm the importance of this residue in triggering the superoxidation process. Indeed, the deprotonation of Glu76 elicits the movement of the unique ferrous iron. This displacement is facilitated by the unusual localized electronic structure of the proximal cluster, which is maintained in the different redox states, thus preserving a low redox potential gap between the two oxidation events.

In conclusion, the asymmetry of the proximal cluster facilitates 1) the mobility of one specific ferrous ion, which in turn induces amide deprotonation, and 2) the full valence localization in all redox states, thus resulting in facile superoxidation. Conversely, proximal [4Fe4S] clusters in O_2-sensitive hydrogenases are compact and rigid, and their full electronic delocalization forbids two successive redox events. Our understanding of the intrinsic properties of the peculiar O_2-tolerant [NiFe]-hydrogenase-proximal FeS cluster should help future efforts in the synthesis of H_2 catalysts with improved performances under oxic conditions.

Received: November 12, 2012
Published online: January 7, 2013

Keywords: hydrogenases · iron–sulfur cluster · redox chemistry · superoxidation

[1] J. C. Fontecilla-Camps, P. Amara, C. Cavazza, Y. Nicolet, A. Volbeda, *Nature* **2009**, *460*, 814 – 822.
[2] A. K. Jones, E. Sillery, S. P. J. Albracht, F. A. Armstrong, *Chem. Commun.* **2002**, 866 – 867.
[3] B. Friedrich, J. Fritsch, O. Lenz, *Curr. Opin. Biotechnol.* **2011**, *22*, 358 – 364.
[4] M. Ludwig, J. A. Cracknell, K. A. Vincent, F. A. Armstrong, O. Lenz, *J. Biol. Chem.* **2009**, *284*, 465 – 477.
[5] M. J. Lukey, A. Parkin, M. M. Roessler, B. J. Murphy, J. Harmer, T. Palmer, F. Sargent, F. A. Armstrong, *J. Biol. Chem.* **2010**, *285*, 3928 – 3938.
[6] M. E. Pandelia, V. Fourmond, P. Tron-Infossi, E. Lojou, P. Bertrand, C. Leger, M. T. Giudici-Orticoni, W. Lubitz, *J. Am. Chem. Soc.* **2010**, *132*, 6991 – 7004.
[7] K. A. Vincent, J. A. Cracknell, J. R. Clark, M. Ludwig, O. Lenz, B. Friedrich, F. A. Armstrong, *Chem. Commun.* **2006**, 5033 – 5035.
[8] a) A. Volbeda, M. H. Charon, C. Piras, E. C. Hatchikian, M. Frey, J. C. Fontecilla-Camps, *Nature* **1995**, *373*, 580 – 587; b) J. C. Fontecilla-Camps, A. Volbeda, C. Cavazza, Y. Nicolet, *Chem. Rev.* **2007**, *107*, 4273 – 4303.
[9] A. Volbeda, L. Martin, C. Cavazza, M. Matho, B. W. Faber, W. Roseboom, S. P. J. Albracht, E. Garcin, M. Rousset, J. C. Fontecilla-Camps, *J. Biol. Inorg. Chem.* **2005**, *10*, 239 – 249.
[10] M. Saggu, I. Zebger, M. Ludwig, O. Lenz, B. Friedrich, P. Hildebrandt, F. Lendzian, *J. Biol. Chem.* **2009**, *284*, 16264 – 16276.

[11] J. Fritsch, S. Loscher, O. Sanganas, E. Siebert, I. Zebger, M. Stein, M. Ludwig, A. L. De Lacey, H. Dau, B. Friedrich, O. Lenz, M. Haumann, *Biochemistry* **2011**, *50*, 5858 – 5869.
[12] K. Knüttel, K. Schneider, A. Erkens, W. Plass, A. Muller, E. Bill, A. X. Trautwein, *Bull. Pol. Acad. Sci. Chem.* **1994**, *42*, 495 – 511.
[13] M. E. Pandelia, W. Nitschke, P. Infossi, M. T. Giudici-Orticoni, E. Bill, W. Lubitz, *Proc. Natl. Acad. Sci. USA* **2011**, *108*, 6097 – 6102.
[14] M. M. Roessler, R. M. Evans, R. A. Davies, J. Harmer, F. A. Armstrong, *J. Am. Chem. Soc.* **2012**, *134*, 15581 – 15594.
[15] a) R. Cammack, *Biochem. Biophys. Res. Commun.* **1973**, *54*, 548 – 554; b) H. A. Heering, Y. B. M. Bulsink, W. R. Hagen, T. E. Meyer, *Eur. J. Biochem.* **1995**, *232*, 811 – 817.
[16] a) T. Goris, A. F. Wait, M. Saggu, J. Fritsch, N. Heidary, M. Stein, I. Zebger, F. Lendzian, F. A. Armstrong, B. Friedrich, O. Lenz, *Nat. Chem. Biol.* **2011**, *7*, 310 – 318; b) M. J. Lukey, M. M. Roessler, A. Parkin, R. M. Evans, R. A. Davies, O. Lenz, B. Friedrich, F. Sargent, F. A. Armstrong, *J. Am. Chem. Soc.* **2011**, *133*, 16881 – 16892.
[17] Y. Shomura, K. S. Yoon, H. Nishihara, Y. Higuchi, *Nature* **2011**, *479*, 253 – 256.
[18] J. Fritsch, P. Scheerer, S. Frielingsdorf, S. Kroschinsky, B. Friedrich, O. Lenz, C. M. T. Spahn, *Nature* **2011**, *479*, 249 – 252.
[19] A. Volbeda, P. Amara, C. Darnault, J. M. Mouesca, A. Parkin, M. M. Roessler, F. A. Armstrong, J. C. Fontecilla-Camps, *Proc. Natl. Acad. Sci. USA* **2012**, *109*, 5305 – 5310.
[20] a) H. M. Senn, W. Thiel, *Atomistic Approaches in Modern Biology: from Quantum Chemistry to Molecular Simulations*, *Vol. 268*, Springer, Berlin, **2007**, pp. 173 – 290; b) H. Lin, D. G. Truhlar, *Theor. Chem. Acc.* **2007**, *117*, 185 – 199.
[21] R. K. Szilagyi, M. A. Winslow, *J. Comput. Chem.* **2006**, *27*, 1385 – 1397.
[22] Y. Zhao, D. G. Truhlar, *Theor. Chem. Acc.* **2008**, *120*, 215 – 241.
[23] H. Sigel, R. B. Martin, *Chem. Rev.* **1982**, *82*, 385 – 426.
[24] O. V. Nemirovskiy, M. L. Gross, *J. Am. Soc. Mass Spectrom.* **1996**, *7*, 977 – 980.
[25] K. Grubel, P. L. Holland, *Angew. Chem.* **2012**, *124*, 3364 – 3366; *Angew. Chem. Int. Ed.* **2012**, *51*, 3308 – 3310.
[26] H. Ogata, P. Kellers, W. Lubitz, *J. Mol. Biol.* **2010**, *402*, 428 – 444.
[27] F. Capozzi, S. Ciurli, C. Luchinat, *Struct. Bonding (Berlin)* **1998**, *90*, 127 – 160.
[28] M. Rousset, Y. Montet, B. Guigliarelli, N. Forget, M. Asso, P. Bertrand, J. C. Fontecilla-Camps, E. C. Hatchikian, *Proc. Natl. Acad. Sci. USA* **1998**, *95*, 11625 – 11630.
[29] a) E. M. Walters, R. Garcia-Serres, G. N. L. Jameson, D. A. Glauser, F. Bourquin, W. Manieri, P. Schurmann, M. K. Johnson, B. H. Huynh, *J. Am. Chem. Soc.* **2005**, *127*, 9612 – 9624; b) A. Dey, E. J. Francis, M. W. W. Adams, E. Babini, Y. Takahashi, K. Fukuyama, K. O. Hodgson, B. Hedman, E. I. Solomon, *Science* **2007**, *318*, 1464 – 1468; c) M. Orio, J. M. Mouesca, *Inorg. Chem.* **2008**, *47*, 5394 – 5416.
[30] J. M. Mouesca, J. L. Chen, L. Noodleman, D. Bashford, D. A. Case, *J. Am. Chem. Soc.* **1994**, *116*, 11898 – 11914.
[31] J. M. Mouesca, B. Lamotte, *Coord. Chem. Rev.* **1998**, *178*, 1573 – 1614.
[32] M. E. Pandelia, P. Infossi, M. Stein, M. T. Giudici-Orticoni, W. Lubitz, *Chem. Commun.* **2012**, *48*, 823 – 825.
[33] M. Schlangen, H. Schwarz, *Helv. Chim. Acta* **2008**, *91*, 379 – 386.
[34] P. L. Tremblay, D. R. Lovley, *J. Bacteriol.* **2012**, *194*, 2248 – 2253.
[35] M. V. Coppi, *Microbiology* **2005**, *151*, 1239 – 1254.